BLACK HOLES

A stellar dynamical mass measurement of an inactive black hole at redshift 2

Andrew B. Newman[1,2]*, Meng Gu[3]†‡, Sirio Belli[4], Richard S. Ellis[5], Sai Gangula[2,1], Jenny E. Greene[6], Jonelle L. Walsh[7,8], Sherry H. Suyu[9,10], Sebastian Ertl[10,9], Gabriel Caminha[10,9], Giovanni Granata[11,12,13], Claudio Grillo[11,14], Stefan Schuldt[11,14]§¶, Tania M. Barone[15], Simeon Bird[16], Karl Glazebrook[15], Marziye Jafariyazani[17,18], Mariska Kriek[19], Allison Matthews[1], Takahiro Morishita[20]#, Themiya Nanayakkara[15], Justin D. R. Pierel[21], Ana Acebrón[22,14], Pietro Bergamini[11,23], Sangjun Cha[24], Jose M. Diego[22], Nicholas Foo[25], Brenda Frye[26], Yoshinobu Fudamoto[27,26], M. James Jee[24,28], Patrick S. Kamieneski[25]**, Anton M. Koekemoer[21], Asish K. Meena[29]††, Shun Nishida[30], Masamune Oguri[27,30], Piero Rosati[12,23], Adi Zitrin[29]

Supermassive black holes and their host galaxies grow together over time, producing correlations between the black hole mass and various galaxy properties. Determining the evolution of these correlations requires precise measurements of the masses of distant black holes. We observed the gravitationally lensed quiescent galaxy MRG-M0138 at redshift 1.95 using James Webb Space Telescope integral field spectroscopy to spatially resolve the kinematics of stars within the black hole's sphere of influence. By using a foreground lens model and fitting stellar dynamical models, we determined the mass of its inactive black hole to be $M_\bullet = 6.0^{+2.1}_{-1.7} \times 10^9$ solar masses. Comparing this measurement to local galaxies, we found that $M_\bullet$ is higher than expected given the galaxy's bulge mass but consistent with the correlation of $M_\bullet$ with stellar velocity dispersion.

The growth of supermassive black holes is intertwined with the growth of their host galaxies. Observations have shown that black hole mass $M_\bullet$ correlates with various host galaxy properties, such as bulge mass and stellar velocity dispersion (*1*–*3*). It is unclear whether these correlations evolved over the history of the Universe.

The masses of distant black holes have been estimated in active galactic nuclei (AGNs), where accretion onto the black hole powers substantial energy output. The accreting material irradiates fast-moving gas clouds surrounding the AGN, known as the broad-line region, enabling the kinematics to be measured if the viewing angle is favorable. The angular size of the broad-line region at redshifts $z \gtrsim 2$ is ~100 micro–arc sec or less, which has been spatially resolved in only two cases (*4*, *5*). Most measurements instead apply mass estimators to emission line widths and luminosities that were measured using unresolved spectra (*6*). However, this approach relies on estimates of the size and structure of the broad-line region, resulting in large uncertainties of up to an order of magnitude (*4*, *5*, *7*).

Measuring the properties of the host galaxies of AGNs is also challenging, especially for the most massive black holes in the distant Universe. Those black holes are found by identifying quasars, luminous AGNs that greatly outshine the stars in their host galaxies. By contrast, observing galaxies with inactive black holes permits both an investigation of the host galaxy properties and a robust measurement of the black hole mass using stellar dynamics. At $z \gtrsim 0.3$, these observations require an angular resolution of tens of milli–arc seconds or better to resolve the black hole's sphere of influence, the region within which the motions of stars are strongly influenced by the gravitational potential of the black hole. Consequently, precise black hole mass measurements are limited to distances <200 Mpc (*8*). This limitation could potentially be overcome if the sphere of influence is highly magnified by gravitational lensing.

Observations and host galaxy properties

The quiescent galaxy MRG-M0138, at $z = 1.95$ (*9*), is highly magnified by gravitational lensing caused by the foreground galaxy cluster MACS J0138.0–2155 (Fig. 1A). The galaxy is intrinsically luminous and dominated by an old stellar population with minimal dust extinction, which enables precise stellar kinematic measurements.

We used the James Webb Space Telescope (JWST) to observe one of the five multiple images of MRG-M0138 at right ascension $1^h38^m03^s.17$, declination $-21°55'47''.6$ (J2000 equinox). The observations used the integral field unit (IFU) of the Near Infrared Spectrograph (NIRSpec) (*10*) with two gratings, which together cover the rest-frame wavelengths $\lambda_{rest} = 0.33$ to 1.07 μm at a resolving power of $R \sim 1000$. We also analyzed images obtained using the Advanced Camera for Surveys on the Hubble Space Telescope (HST) and the Near-Infrared Camera (NIRCam) on JWST, which span $\lambda_{rest} = 0.19$ to 1.5 μm in seven filters (*11*).

We interpreted the observations using a model of the gravitational lens (*12*). We used the results of seven independently constructed lens models to estimate uncertainties in the magnification $\mu = 29^{+13}_{-11}$ (*13*) and its anisotropy (*11*). Given this magnification, the point spread function (PSF) of the IFU observations is equivalent to a spatial resolution of $\sigma_{psf} = 91^{+41}_{-35}$ pc at the distance of MRG-M0138 (*11*).

We reconstructed the NIRCam images in the source plane (Fig. 1B), which show that the galaxy has a multicomponent structure: An inclined disk contributes 62% of the light at $\lambda_{rest} \approx 0.68$ μm, with the remainder from a compact stellar bulge. We extracted spectra from the IFU data cube in 219 spatial bins [not all independent (*11*)] along with matched photometry from the seven images. We used stellar population synthesis (SPS) techniques to model the spectra and photometry, producing maps of the stellar velocity V (Fig. 1C), stellar velocity dispersion σ (Fig. 1D), and the stellar mass and light distributions (fig. S5).

[1]Observatories, Carnegie Institution for Science, Pasadena, CA, USA. [2]Department of Physics and Astronomy, University of Southern California, Los Angeles, CA, USA. [3]Department of Physics, The University of Hong Kong, Hong Kong, China. [4]Dipartimento di Fisica e Astronomia, Università di Bologna, Bologna, Italy. [5]Department of Physics & Astronomy, University College London, London, UK. [6]Department of Astrophysical Sciences, Princeton University, Princeton, NJ, USA. [7]George P. and Cynthia Woods Mitchell Institute for Fundamental Physics and Astronomy, Texas A&M University, College Station, TX, USA. [8]Department of Physics and Astronomy, Texas A&M University, College Station, TX, USA. [9]School of Natural Sciences, Technical University of Munich, Garching, Germany. [10]Max-Planck-Institut für Astrophysik, Garching, Germany. [11]Dipartimento di Fisica, Università degli Studi di Milano, Milano, Italy. [12]Dipartimento di Fisica e Scienze della Terra, Università degli Studi di Ferrara, Ferrara, Italy. [13]Institute of Cosmology and Gravitation, University of Portsmouth, Portsmouth, UK. [14]Instituto di Astrofisica Spaziale e Fisica cosmica Milano, Istituto Nazionale di Astrofisica, Milano, Italy. [15]Centre for Astrophysics and Supercomputing, Swinburne University of Technology, Hawthorn, Victoria, Australia. [16]Department of Physics & Astronomy, University of California Riverside, Riverside, CA, USA. [17]SETI Institute, Mountain View, CA, USA. [18]NASA Ames Research Center, Moffett Field, CA, USA. [19]Leiden Observatory, Leiden University, Leiden, Netherlands. [20]Infrared Processing and Analysis Center, California Institute of Technology, Pasadena, CA, USA. [21]Space Telescope Science Institute, Baltimore, MD, USA. [22]Instituto de Física de Cantabria, Santander, Spain. [23]Osservatorio di Astrofisica e Scienza dello Spazio di Bologna, Istituto Nazionale di Astrofisica, Bologna, Italy. [24]Department of Astronomy, Yonsei University, Seoul, Korea. [25]School of Earth and Space Exploration, Arizona State University, Tempe, AZ, USA. [26]Department of Astronomy and Steward Observatory, University of Arizona, Tucson, AZ, USA. [27]Center for Frontier Science, Chiba University, Chiba, Japan. [28]Department of Physics and Astronomy, University of California Davis, Davis, CA, USA. [29]Department of Physics, Ben-Gurion University of the Negev, Be'er-Sheva, Israel. [30]Department of Physics, Graduate School of Science, Chiba University, Chiba, Japan. ***Corresponding author. Email: anewman@carnegiescience.edu** †Present address: Department of Astronomy, Tsinghua University, Beijing, China. ‡Present address: Hong Kong Institute for Astronomy & Astrophysics, The University of Hong Kong, Hong Kong, China. §Present address: Finnish Centre for Astronomy with the European Southern Observatory, Turku, Finland. ¶Present address: Department of Physics, University of Helsinki, Helsinki, Finland. #Present address: Astronomical Institute, Tohoku University, Sendai, Japan. **Present address: Department of Space, Earth & Environment, Chalmers University of Technology, Gothenburg, Sweden. ††Present address: Department of Physics, Indian Institute of Science, Bengaluru, India.

We found that MRG-M0138 is a massive and dense galaxy, with total stellar mass $M_{*,\mathrm{MW}} = 2.2^{+1.4}_{-0.7} \times 10^{11}$ solar masses ($M_\odot$), assuming the same stellar initial mass function (IMF) as the Milky Way (*14*). It has an effective radius (the half-light semimajor axis) of $R_\mathrm{e} = 2.73^{+0.77}_{-0.46}$ kpc, which is typical of quiescent galaxies at this mass and redshift (*15*). It also has a high effective velocity dispersion $\sigma_\mathrm{e} = 398 \pm 12$ km s^{-1}, which we define as the second velocity moment $V_\mathrm{rms} = \sqrt{V^2 + \sigma^2}$ averaged within the bulge effective radius, $R_\mathrm{e,bulge} = 0.83^{+0.23}_{-0.14}$ kpc, where the subscript "rms" represents "root mean square," and the uncertainties were derived from the estimated systematic effects (*11*).

Black hole mass and Eddington ratio

We modeled the stellar dynamics of the host galaxy using Jeans anisotropic modeling (*16*), a technique that has been verifed for determining $M_\bullet$ estimates in fast-rotating galaxies (*17*) similar to MRG-M0138. We constructed flexible dynamical models to estimate $M_\bullet$ after marginalizing over a range of stellar mass distributions, velocity anisotropies, and inclinations (*11*). Our initial estimates of the stellar mass distributions of the bulge and disk relied on the SPS model fitting, which allowed for gradients in stellar population age, metallicity (abundance of elements heavier than helium), and dust but assumed a Milky Way IMF. The dynamical models permit this initial stellar mass distribution to vary, thereby allowing for the possibility of a non–Milky Way IMF with spatial gradients. The small gas mass in MRG-M0138 (*18*) is dynamically negligible (*11*). The dynamical models also include dark matter, a central black hole, and gradients in the velocity anisotropy.

The dynamical models were fitted to the observed V_rms map (Fig. 2). We considered six model variations to test the influence of both the uncertain IMF and its possible spatial gradients as well as the assumed orientation of the stellar velocity ellipsoid, which describes the anisotropy of the velocity dispersion (*11*). All six model variations produce consistent estimates of $M_\bullet$ (fig. S6). We combined these estimates using Bayesian model averaging, finding $\log(M_\bullet/M_\odot) = 9.78^{+0.08}_{-0.12}(1\sigma\ \mathrm{stat.})^{+0.11}_{-0.09}(\mathrm{sys.})$; combining the statistical and systematic uncertainties in quadrature gives $\log(M_\bullet/M_\odot) = 9.78^{+0.13}_{-0.15}$. Among the six dynamical models, we selected a fiducial model as the basis for estimating systematic uncertainties and performing the tests described below. The largest contribution to the systematic uncertainty is the lensing magnification (*11*). The radius of the black hole sphere of influence, $r_\mathrm{inf} = 164$ pc, is marginally spatially resolved, by a factor of $r_\mathrm{inf}/\sigma_\mathrm{psf} = 1.8$, which is similar to that achieved in observations of nearby black holes with lower masses (*17*). The fitted dynamical mass of the stellar bulge is $M_\mathrm{bulge} = 1.03^{+0.33}_{-0.22} \times 10^{11} M_\odot$ and the total dynamical stellar mass is $M_\mathrm{stars} = 2.54^{+0.87}_{-0.55} \times 10^{11} M_\odot$ (uncertainties are combined 1σ statistical and systematic components).

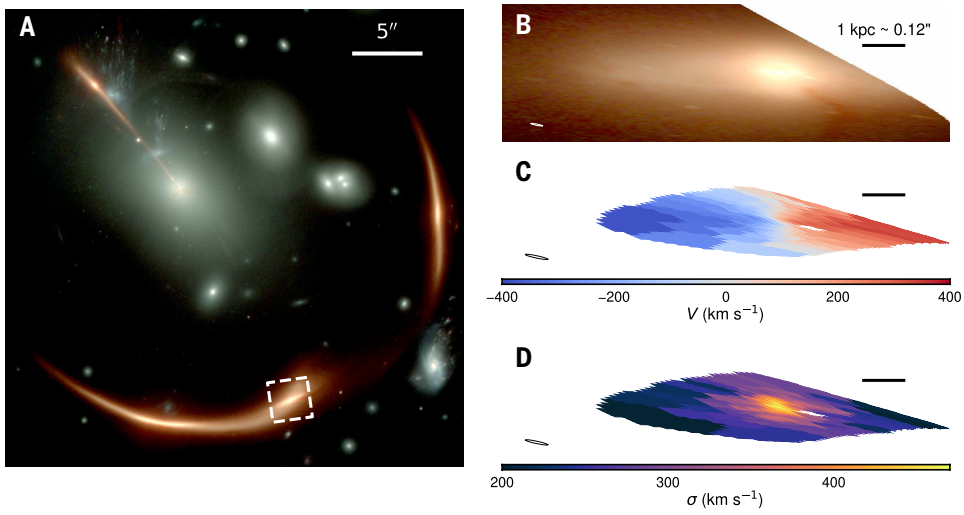

Fig. 1. Morphology and stellar kinematics of MRG-M0138. (**A**) JWST/NIRCam image of the foreground galaxy cluster MACS J0138.0–2155 through the F115W (blue), F150W (green), and F356W (red) filters, displayed with a logarithmic brightness stretch. The bright red arcs are multiple images of MRG-M0138 produced by gravitational lensing. The dashed box shows the field of view of the NIRSpec IFU used in our observations. (**B**) Reconstructed image of the galaxy in the source plane after removing the effect of gravitational lensing. The white ellipse represents the effective PSF. (**C**) Same region as in (B), colored to indicate the stellar velocity V derived from the NIRSpec IFU data. (**D**) Same as (C), but the color indicates the stellar velocity dispersion σ.

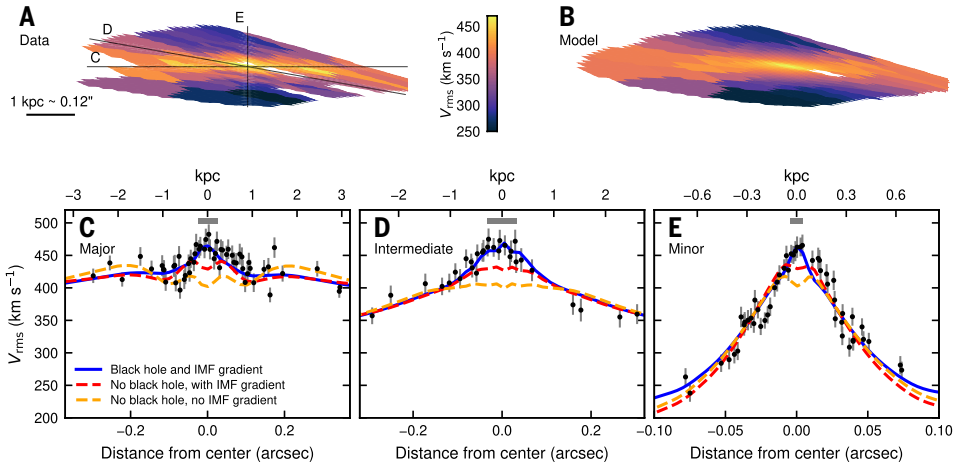

Fig. 2. The black hole mass constrained by stellar dynamical models. (**A**) Same as Fig. 1D but showing the second velocity moment V_rms (color bar). Labeled lines indicate the directions along which kinematics are displayed in (C) to (E). (**B**) The corresponding V_rms map produced by the best-fitting fiducial dynamical model, which includes a black hole. (**C**) The kinematics along the major axis of the galaxy. Colored lines indicate the fiducial model, which includes a black hole and a radial IMF gradient (blue solid line), a similar model that lacks a black hole (red dashed line), and a model that includes neither a black hole nor a radial IMF gradient (orange dashed line). The models are described in the supplementary materials. The gray scale bar indicates the width of the PSF. Corrections were applied to the observed data to remove distortions caused by spatial binning (*11*). (**D**) Same as (C) but showing kinematics along an intermediate axis, which makes a 45° angle with the major and minor axes when deprojected. (**E**) Same as (C) but for the minor axis. The two models without a black hole do not match the central peak in V_rms [(C) to (E)].

We also considered several dynamical models that omit a black hole. These models do not match the central V_rms peak in the observations (Fig. 2, C to E, and fig. S8), even if an IMF gradient is allowed to increase the central mass density. Compared with the fiducial dynamical model that includes a black hole, the models with no black hole are disfavored by Bayes factors ranging from 735 to 8×10^{12}. As a further test, we replaced the black hole in the fiducial dynamical model with an extended dark mass with a free mass, size, and shape. We found that the kinematics require that the dark mass is spatially unresolved, setting a limit on its radius of <28 pc (95% confidence) (fig. S9), which is close to the source plane spatial resolution of the IFU data in the most-magnified direction. The required

surface density within this radius is $10^{6.8\pm0.4} M_\odot$ pc^{-2}, which we regard as implausibly high for a stellar system mimicking a black hole (*11*).

We isolated the nuclear spectrum within $r \approx 100$ pc of the galaxy center to place limits on any AGN activity. Faint emission lines of singly ionized nitrogen and oxygen ([N II] and [O II]) were detected (fig. S10), and upper limits were placed on emission from hydrogen (Hα) and doubly ionized oxygen ([O III]). The flux ratios are log([N II]/Hα) > 0.75 and log([O III]/[O II]) < −0.10 (2σ limits), consistent with the presence of a low-ionization nuclear emission region (LINER). The upper limit on Hα emission constrains the AGN bolometric luminosity $L_{\rm bol} < 10^{42.8}$ erg s^{-1} (*11*). The resulting Eddington ratio, the ratio of $L_{\rm bol}$ to a theoretical maximum Eddington luminosity, is $\lambda_{\rm Edd} < 10^{-5.1}$ (*11*). Both of these upper limits include the statistical 2σ range and systematic uncertainties. No x-ray emission from this galaxy was detected in an archival observation by the Chandra X-ray Observatory, which provides a consistent (but 0.6 dex weaker) limit on $L_{\rm bol}$ (*11*). MRG-M0138 therefore has a similarly low Eddington ratio as that of typical local galaxies not classified as AGN, where the most common mode of accretion is expected to be inefficient at producing radiation (*19*). Figure 3A compares our limit on $L_{\rm bol}$ in MRG-M0138 with measurements of galaxies in the local Universe and galaxies at $z > 1$ with previous $M_\bullet$ measurements based on broad emission lines; the latter all have $\lambda_{\rm Edd} \gtrsim 0.01$.

Black hole scaling relations

Our results indicate that the black hole in MRG-M0138 is as massive as those in quasars (Fig. 3A). Quasars are identified based on their high bolometric luminosities; this preferentially selects the most massive black holes and makes it difficult to infer the evolution of the galaxy–black hole correlations (*20*). By contrast, stellar dynamical methods allow measurements of $M_\bullet$ in inactive galaxies, such as MRG-M0138, circumventing this type of selection bias. We found that the black hole mass fraction $M_\bullet/M_{\rm stars} = 0.024^{+0.008}_{-0.007}$ of MRG-M0138 is an order of magnitude higher than the average black hole mass fraction of faint AGN at the same redshift (*21*). It is also near the top of the range of $M_\bullet/M_{\rm stars}$ ratios typically observed in local early-type (elliptical and lenticular) or late-type (spiral) galaxies (Fig. 2B).

Most cosmological simulations do not produce $z = 2$ galaxies with both the $M_\bullet$ and $M_{\rm stars}$ that we measured for MRG-M0138 (*22*). For example, the Astrid simulation contains 635 galaxies at $z = 2$ that match the stellar mass of MRG-M0138 (within 1σ), but only 2 contain a black hole at least as massive (within 1σ or above) (*23*). The semiempirical model TRINITY predicts the median $M_\bullet - M_{\rm stars}$ relation at $z = 2$ (*24*), and the black hole in MRG-M0138 is a factor of five above it, a difference of 2.6 standard deviations (our measurement uncertainty added in quadrature to the intrinsic scatter predicted by TRINITY). Our results are consistent with previous indications that early black hole growth was very efficient in at least some galaxies (*25*–*27*).

The origin of the high $M_\bullet$ in MRG-M0138 could be related to the galaxy density, as indicated by the very high value of σ_e. MRG-M0138 is consistent with the local $M_\bullet - \sigma_e$ relation (Fig. 3D). Previous studies of high-redshift galaxies that used gas emission lines as proxies for σ_e (*28*) were also consistent with the local relation, implying that it does not strongly evolve. This result informs uncertain models of black hole growth; cosmological simulations predict a wide range in the amount of evolution in the $M_\bullet - \sigma_e$ relation (*29*, *30*). Our measurement also indirectly supports some previous broad-line $M_\bullet$ estimates at $z > 2$: If the $M_\bullet - \sigma_e$ relation has negligible evolution, σ_e can be used to estimate $M_\bullet$ at those redshifts. The resulting estimate is consistent with broad-line estimates (*31*, *32*) in two quiescent galaxies at $z \approx 2$ and 5 (Fig. 3D).

By contrast, MRG-M0138 lies above the $M_\bullet - M_{\rm bulge}$ relation of local early-type galaxies (*1*) by a factor of 12 (Fig. 3C), a difference of 3.3 standard deviations (our measurement uncertainty added in quadrature to the intrinsic scatter). If MRG-M0138 is typical of galaxies at $z \sim 2$, then it indicates that the $M_\bullet - M_{\rm bulge}$ relation has evolved much more than the $M_\bullet - \sigma_e$ relation. This is probably because galaxies underwent substantial morphological change, including bulge growth, after the main period of star formation and black hole growth (*33*). Similar conclusions on the evolution of the $M_\bullet - M_{\rm bulge}$ relation have been reached by studies of quasar hosts using statistical estimates of $M_{\rm bulge}$ (*34*).

Possible evolutionary pathways

The dominant growth mechanism for the black hole in MRG-M0138 was probably accretion during optically luminous quasar phases (*35*). If it grew at $\lambda_{\rm Edd} \sim 0.3$, which is typical of quasars (*36*), its AGN luminosity would have been $L_{\rm bol} \approx 10^{47}$ erg s^{-1}. Quasars with such luminosities often drive winds that eject gas at outflow rates of $\sim 10^3\, M_\odot$ yr^{-1} (*37*). Our $M_\bullet$ measurement therefore indicates that MRG-M0138 was likely a site of powerful AGN feedback. We cannot demonstrate a causal link between that feedback and the quenching of star formation in MRG-M0138 or its low gas fraction. However, this scenario is consistent with theoretical models that produce massive elliptical galaxies from a merger-induced starburst

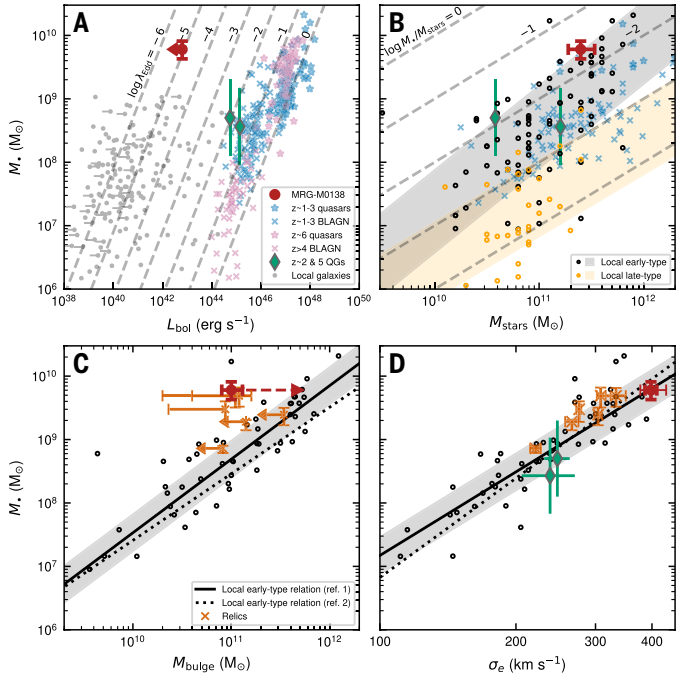

Fig. 3. Comparison of MRG-M0138 to galaxy–black hole scaling relations. Data sources are listed in table S3. (**A**) Black hole mass as a function of AGN luminosity $L_{\rm bol}$. The gray dashed lines are logarithmically spaced values of the Eddington ratio. Our measurements of MRG-M0138 are shown with the red circle; the upper limit on $L_{\rm bol}$ includes the statistical 2σ range and systematic uncertainties. Other data points indicate observational measurements of quasars at $z \sim 1$ to 3 (blue stars) and $z \sim 6$ (pink stars), broad-line AGN (BLAGN) at $z \sim 1$ to 3 (blue crosses) and $z > 4$ (pink crosses), two quiescent galaxies (QGs) at $z \sim 2$ and 5 with BLAGN (green diamonds), and a sample of local galaxies (gray dots; attached lines indicate 3σ upper limits). (**B**) The black hole mass as a function of total stellar mass $M_{\rm stars}$. Gray dashed lines show logarithmically spaced values of the mass ratio $M_\bullet/M_{\rm stars}$. The red circle represents MRG-M0138, which is compared to local early-type (black circles) and late-type (orange circles) galaxies with dynamically determined $M_\bullet$ [shaded bands show the scaling relations previously fitted to those data sets (*3*)] and $z \gtrsim 1$ galaxies [symbols are the same as in (A)]. (**C**) The black hole mass as a function of bulge stellar mass $M_{\rm bulge}$. Black circles represent local early-type galaxies, and black lines represent scaling relations previously derived from observations [solid line with shaded band showing the 1σ scatter (*1*), dashed line (*2*)]. Oranges crosses represent local relic galaxies, with error bars on $M_{\rm bulge}$ encompassing a range of morphological decompositions and upper limits (arrows) shown if only the total stellar mass is plotted. The dashed red arrow indicates our estimated evolution of MRG-M0138. (**D**) Black hole mass as a function of effective stellar velocity dispersion σ_e. Symbols are the same as in (A) and (C). Thin error bars on MRG-M0138 encompass a range of σ_e definitions (*11*). Except where otherwise specified, error bars indicate 1σ uncertainties. Further details on the construction of this figure are provided in the supplementary materials.

and quasar phase (*38*). A major merger would have destroyed the stellar disks of the progenitors, but that is not incompatible with the thin stellar disk in MRG-M0138 (*33*). Simulations of major mergers predict that if the gas fraction is as high as observed at $z \gtrsim 2$ (*39*), then a substantial fraction of the gas is not consumed by the postmerger starburst and instead reforms a gas disk, where star formation can continue (*40*, *41*).

MRG-M0138 will likely become an elliptical galaxy by $z \sim 0$: Its mass is $M_{\rm stars} \approx 10^{11.4}\,M_{\odot}$, which we expect to double between $z = 2$ and 0, primarily owing to mergers (*42*). At $z \sim 0$, this mass regime is dominated by slowly rotating, elliptical galaxies (*43*). If these later mergers are gas-poor, then they would cause little black hole growth (*44*) and only modest changes to σ_e (*45*). MRG-M0138 would remain consistent with the local $M_\bullet - \sigma_e$ relation (fig. 3D) but evolve toward the mean $M_\bullet - M_{\rm stars}$ relation (Fig. 3B) of early-type galaxies. To form an elliptical galaxy, the mergers must redistribute stars from the stellar disk into a bulge; along with the expected mass doubling, this evolution would bring MRG-M0138 onto the local $M_\bullet - M_{\rm bulge}$ relation (Fig. 3C), producing black hole and stellar masses similar to those of the nearby elliptical galaxy Messier 87 (*46*, *47*).

A rare class of galaxies in the local Universe, known as relics, have been interpreted as the descendants of galaxies that quenched at $z \gtrsim 2$ and experienced no major mergers afterward, thereby surviving intact to $z \sim 0$ (*48*). We tested this interpretation by comparing the resolved stellar kinematics and $M_\bullet$ of MRG-M0138 to those of the relic galaxies. The rapidly rotating disk and peaked central velocity dispersion of MRG-M0138 (Fig. 1, C and D) resemble the kinematics of relic galaxies (*49*, *50*). Stellar dynamical models indicate that the relic galaxies, such as MRG-M0138, are outliers on the $M_\bullet - M_{\rm bulge}$ relation but not the $M_\bullet - \sigma$ relation (*51*–*53*) (Figs. 2, C and D). Our results therefore support the interpretation of relic galaxies as being undisturbed descendants of early quiescent galaxies.

REFERENCES AND NOTES

1. J. Kormendy, L. C. Ho, *Annu. Rev. Astron. Astrophys.* **51**, 511–653 (2013).
2. N. J. McConnell, C.-P. Ma, *Astrophys. J.* **764**, 184 (2013).
3. J. E. Greene, J. Strader, L. C. Ho, *Annu. Rev. Astron. Astrophys.* **58**, 257–312 (2020).
4. R. Abuter *et al.*, *Nature* **627**, 281–285 (2024).
5. K. Abd El Dayem *et al.*, *Astron. Astrophys.* **706**, A99 (2026).
6. J. E. Greene, L. C. Ho, *Astrophys. J.* **630**, 122–129 (2005).
7. C. Bertemes *et al.*, *Astron. Astrophys.* **693**, A176 (2025).
8. K. Mehrgan *et al.*, *Astrophys. J.* **887**, 195 (2019).
9. A. B. Newman, S. Belli, R. S. Ellis, S. G. Patel, *Astrophys. J.* **862**, 125 (2018).
10. P. Jakobsen *et al.*, *Astron. Astrophys.* **661**, A80 (2022).
11. Materials and methods are available as supplementary material.
12. S. Ertl *et al.*, *Astron. Astrophys.* **702**, A157 (2025).
13. S. H. Suyu *et al.*, *Astron. Astrophys.* **708**, A291 (2026).
14. P. Kroupa, *Mon. Not. R. Astron. Soc.* **322**, 231–246 (2001).
15. A. van der Wel *et al.*, *Astrophys. J.* **788**, 28 (2014).
16. M. Cappellari, *Mon. Not. R. Astron. Soc.* **390**, 71–86 (2008).
17. S. Thater *et al.*, *Astron. Astrophys.* **625**, A62 (2019).
18. K. E. Whitaker *et al.*, *Nature* **597**, 485–488 (2021).
19. L. C. Ho, *Astrophys. J.* **699**, 626–637 (2009).
20. T. R. Lauer, S. Tremaine, D. Richstone, S. M. Faber, *Astrophys. J.* **670**, 249–260 (2007).
21. H. Suh *et al.*, *Astrophys. J.* **889**, 32 (2020).
22. M. Habouzit *et al.*, *Mon. Not. R. Astron. Soc.* **503**, 1940–1975 (2021).
23. Y. Ni *et al.*, *Astrophys. J.* **990**, 120 (2025).
24. H. Zhang *et al.*, *Mon. Not. R. Astron. Soc.* **518**, 2123–2163 (2023).
25. A. D. Goulding *et al.*, *Astrophys. J. Lett.* **955**, L24 (2023).
26. I. Juodžbalis *et al.*, *Nature* **636**, 594–597 (2024).
27. M. Yue *et al.*, *Astrophys. J.* **966**, 176 (2024).
28. R. Maiolino *et al.*, *Astron. Astrophys.* **691**, A145 (2024).
29. D. Sijacki *et al.*, *Mon. Not. R. Astron. Soc.* **452**, 575–596 (2015).
30. N. Thomas, R. Davé, D. Anglés-Alcázar, M. Jarvis, *Mon. Not. R. Astron. Soc.* **487**, 5764–5780 (2019).
31. A. C. Carnall *et al.*, *Nature* **619**, 716–719 (2023).
32. K. Ito *et al.*, *Mon. Not. R. Astron. Soc.* **538**, 1501–1516 (2025).
33. A. B. Newman, S. Belli, R. S. Ellis, S. G. Patel, *Astrophys. J.* **862**, 126 (2018).
34. X. Ding *et al.*, *Astrophys. J.* **888**, 37 (2020).
35. Q. Yu, S. Tremaine, *Mon. Not. R. Astron. Soc.* **335**, 965–976 (2002).
36. J. A. Kollmeier *et al.*, *Astrophys. J.* **648**, 128–139 (2006).
37. F. Fiore *et al.*, *Astron. Astrophys.* **601**, A143 (2017).
38. P. F. Hopkins, L. Hernquist, T. J. Cox, D. Kereš; Galaxy Mergers and Quasar Activity, *Astrophys. J. Suppl. Ser.* **175**, 356–389 (2008).
39. L. J. Tacconi *et al.*, *Astrophys. J.* **853**, 179 (2018).
40. B. Robertson *et al.*, *Astrophys. J.* **645**, 986–1000 (2006).
41. P. F. Hopkins, T. J. Cox, J. D. Younger, L. Hernquist, *Astrophys. J.* **691**, 1168–1201 (2009).
42. G. B. Brammer *et al.*, *Astrophys. J.* **739**, 24 (2011).
43. E. Emsellem *et al.*, *Mon. Not. R. Astron. Soc.* **414**, 888–912 (2011).
44. A. Kulier, J. P. Ostriker, P. Natarajan, C. N. Lackner, R. Cen, *Astrophys. J.* **799**, 178 (2015).
45. M. Hilz *et al.*, *Mon. Not. R. Astron. Soc.* **425**, 3119–3136 (2012).
46. L. J. Oldham, M. W. Auger, *Mon. Not. R. Astron. Soc.* **457**, 421–439 (2016).
47. K. Akiyama *et al.*, *Astrophys. J. Lett.* **875**, L1 (2019).
48. I. Trujillo, A. Ferré-Mateu, M. Balcells, A. Vazdekis, P. Sánchez-Blázquez, *Astrophys. J. Lett.* **780**, L20 (2014).
49. A. Yıldırım *et al.*, *Mon. Not. R. Astron. Soc.* **452**, 1792–1816 (2015).
50. A. Ferré-Mateu *et al.*, *Mon. Not. R. Astron. Soc.* **467**, 1929–1939 (2017).
51. J. L. Walsh *et al.*, *Astrophys. J.* **808**, 183 (2015).
52. J. L. Walsh *et al.*, *Astrophys. J.* **817**, 2 (2016).
53. J. L. Walsh *et al.*, *Astrophys. J.* **835**, 208 (2017).
54. A. B. Newman, MRG-M0138 Observations, Barbara A. Mikulski Archive for Space Telescopes (2025); https://doi.org/10.17909/ryaj-k740.
55. A. B. Newman, Code and data used to measure the black hole mass in MRG-M0138, Zenodo (2026); https://doi.org/10.5281/zenodo.16767130.

ACKNOWLEDGMENTS

This work is based on observations made with the NASA/European Space Agency/Canadian Space Agency JWST. These observations are associated with programs GO-2345 and DD-6549. The data were obtained from the Mikulski Archive for Space Telescopes at the Space Telescope Science Institute, which is operated by the Association of Universities for Research in Astronomy, Inc., under NASA contract no. NAS 5-03127. This research has made use of data obtained from the Chandra Data Archive provided by the Chandra X-ray Center. A.B.N. performed part of this work at the Aspen Center for Physics, which is supported by National Science Foundation grant no. PHY-2210452. **Funding:** A.B.N. and S.G. received support for program GO-2345 provided by NASA through a grant from the Space Telescope Science Institute. J.D.R.P. and A.B.N. received support for program DD-6549 provided by NASA through a grant from the Space Telescope Science Institute. A.Z. acknowledges support from the United States–Israel Binational Science Foundation grant no. 2020750, the United States National Science Foundation (NSF) grant no. 2109066, and the Israel Science Foundation grant no. 864/23. S.Bi. acknowledges funding from NASA ATP 80NSSC22K1897. R.S.E. acknowledges financial support from the Peter and Patricia Gruber Foundation. M.J.J. acknowledges support for the current research from the National Research Foundation (NRF) of Korea under programs 2022R1A2C1003130 and RS-2023-00219959. S.S. received funding from the European Union's Horizon 2022 research and innovation program under the Marie Skłodowska-Curie grant agreement no 101105167 — FASTIDIoUS. M.O. was supported by JSPS KAKENHI grant no. JP22K21349 and JP25H00662. Y.F. was supported by JSPS KAKENHI grant no. JP23K13149. S.C. was supported by Basic Science Research Program through the NRF of Korea funded by the Ministry of Education (no. RS-2024-00413036). A.A. acknowledges financial support through the Beatriz Galindo program and the project PID2022-138896NB-C51 (MCIU/AEI/MINECO/FEDER, UE), Ministerio de Ciencia, Investigación y Universidades. S.E. and S.H.S. thank the Max Planck Society for support through the Max Planck Fellowship awarded to S.H.S. S.H.S. received funding from the European Research Council (ERC) under the European Union's Horizon 2020 research and innovation program (LENSNOVA: grant no. 771776). S.H.S. and G.C. were supported in part by the Deutsche Forschungsgemeinschaft (German Research Foundation) under Germany's Excellence Strategy – EXC-2094 – 390783311. G.G. acknowledges financial support through grant PRIN-MIUR 2020SKSTHZ. C.G., P.B., and P.R. acknowledge support through grant MIUR2020 SKSTHZ. J.E.G. acknowledges support from NSF AAG grant 2306950. S.Be. was supported by the ERC Starting Grant "Red Cardinal," GA 101076080. J.L.W. acknowledges the support of NSF AST-2206219. K.G. and T.N. acknowledge support from Australian Research Council Laureate Fellowship FL180100060. K.G. and T.M.B. acknowledge support from Australian Research Council Discovery Project DP230101775. **Author contributions:** A.B.N. led the analysis of the source kinematics, stellar populations, and structure; the dynamical modeling; the x-ray analysis; and the drafting of the paper. M.G. reduced the spectroscopic data. A.M. searched for archival data. A.B.N., S.Be., R.S.E., K.G., M.J., M.K., T.N., A.M.K, and J.P. contributed to the acquisition, planning, and execution of the observations. S.Bi. and A.B.N. performed the Astrid comparison. S.H.S., S.E., G.C., G.G., C.G., S.S., A.A., P.B., S.C., J.M.D., N.F., B.F., Y.F., M.J.J., P.S.K., A.K.M., S.N., M.O., P.R., and A.Z. performed calculations based on seven lens models that enabled the source-plane reconstruction and estimation of its uncertainty. All authors contributed to the interpretation of the results and to the writing of the paper. **Competing interests:** The authors declare that they have no competing interests. **Data, code, and materials availability:** The JWST and HST observations are available from the Barbara A. Mikulski Archive for Space Telescopes (MAST) (*54*). Our derived stellar kinematics, lens mapping, and custom analysis code are archived at Zenodo (*55*). No physical materials were generated in this work.

SUPPLEMENTARY MATERIALS

science.org/doi/10.1126/science.adx5816
Materials and Methods; Figs. S1 to S10; Tables S1 to S3; References (*56*–*120*)

Submitted 21 March 2025; accepted 21 April 2026

10.1126/science.adx5816

A stellar dynamical mass measurement of an inactive black hole at redshift 2

Andrew B. Newman, Meng Gu, Sirio Belli, Richard S. Ellis, Sai Gangula, Jenny E. Greene, Jonelle L. Walsh, Sherry H. Suyu, Sebastian Ertl, Gabriel Caminha, Giovanni Granata, Claudio Grillo, Stefan Schuldt, Tania M. Barone, Simeon Bird, Karl Glazebrook, Marziye Jafariyazani, Mariska Kriek, Allison Matthews, Takahiro Morishita, Themiya Nanayakkara, Justin D. R. Pierel, Ana Acebrón, Pietro Bergamini, Sangjun Cha, Jose M. Diego, Nicholas Foo, Brenda Frye, Yoshinobu Fudamoto, M. James Jee, Patrick S. Kamieneski, Anton M. Koekemoer, Asish K. Meena, Shun Nishida, Masamune Oguri, Piero Rosati, and Adi Zitrin

Science **392** (6802), . DOI: 10.1126/science.adx5816

Editor's summary

Most galaxies contain a supermassive black hole at their center. The black hole mass can be determined from stellar kinematics, which requires a high spatial resolution that is usually only available for nearby targets. For more distant galaxies, the black hole mass must be inferred indirectly using empirical scaling relations, but it is unclear whether those are valid beyond the local Universe. Newman *et al*. took advantage of a gravitational lens that magnifies a distant galaxy. This approach provides sufficient spatial resolution to model the stellar kinematics and determine the black hole mass. Its value is consistent with one local scaling relation but inconsistent with another. —Keith T. Smith